Nanoscale

Cite this: *Nanoscale*, 2012, **4**, 1770

www.rsc.org/nanoscale

PAPER

Effects of disorder on the optical properties of CVD grown polycrystalline graphene†

Ramakrishna Podila,[a] Benoy Anand,[b] John T. Spear,[a] P. Puneet,[a] Reji Philip,[c] S. Siva Sankara Sai[b] and Apparao M. Rao*[ad]

Received 29th August 2011, Accepted 29th December 2011
DOI: 10.1039/c2nr11206j

We explore the effects of crystallite size (L_a) on the linear and non-linear optical properties of chemical vapor deposition grown polycrystalline graphene. The π-plasmon resonance present at ~4.75 eV (~260 nm) in the optical absorption spectrum of graphene follows the empirical relationship $\lambda_\pi = 250.5\ \text{nm} + 89.5\ \text{nm}^2/L_a$, where λ_π represents the π-plasmon wavelength. Furthermore, our Z-scan studies reveal that the crystallite size significantly changes the saturation intensity in CVD grown graphene. Notably, in comparison to epitaxial graphene layers grown on SiC wafers which exhibit a photogenerated carrier lifetime of few picoseconds, we find that the photogenerated carriers in our CVD grown graphene can exhibit lifetimes as long as nanoseconds.

Introduction

Graphene is a two-dimensional hexagonal framework of carbon atoms with unique electronic and optical properties. Single layer (SLG) and bi-layer (BLG) graphene[1,2] differ from each other with respect to their electronic band structure: SLG exhibits a conical band structure that converges to a single Dirac point[3] while the AB-stacked BLG possesses massive Dirac fermions with a transverse field-tunable band gap.[4] Such differences in the electronic band structure of SLG, BLG and few layer graphene (FLG) are clearly reflected in their Raman spectra.[5] Depending on the number of layers, the G′-band present at ~2700 cm^{-1} in the Raman spectrum of graphene exhibits a characteristic lineshape. For example, the G′-band in SLG can be fit to a single Lorentzian peak and its integrated area is higher than that of the G-band located at ~1585 cm^{-1}.[6–10] As the number of layers increase (from SLG to highly oriented pyrolytic graphite (HOPG)), the G′-band evolves into a two-peak structure with a concomitant decrease in $I_{G'}/I_G$, where $I_{G'}$ and I_G represent the integrated intensities of the G′- and G-bands, respectively. The Raman spectrum of graphene or nanographite exhibits an additional feature at ~1350 cm^{-1} (known as the D-band) due to the presence of structural disorder in its lattice such as, impurities, edges, hydrogen atoms and finite size effects that break the translational symmetry. The ratio I_D/I_G has also been widely used in the literature for determining the in-plane crystallite size (L_a) for polycrystalline graphite samples.[12–15] L_a serves as an estimate for the average domain length within which the graphene lattice is defect-free. It is important to note that L_a is different from the grain size.

Several fundamental properties of graphene have been discerned from studies using exfoliated single-grain graphene samples[1–6] and the effects of layer stacking (crystallinity perpendicular to the graphene plane) on the optical properties of graphene, such as Raman scattering and linear absorption, are well understood.[6–11] Recently, the chemical vapor deposition (CVD) technique has gained popularity since large area high-quality *polycrystalline* graphene on metallic substrates can be readily prepared using this method. It is well known that L_a significantly influences many physical properties of polycrystalline graphitic materials,[12–16] and thus the presence of grain boundaries in the CVD grown samples is expected to considerably modify the electronic and optical properties of graphene. Presently, there are few studies which describe the effects of in-plane crystallinity (L_a) on the optical properties of graphene. Dawlaty *et al.*[17] found that higher values of L_a (or smaller crystal disorder) in epitaxial graphene prepared on SiC result in long-lived (0.4–1.7 ps) photogenerated carriers in graphene. Based on reflected electron energy loss and Raman spectroscopy, Hashimoto *et al.*[15] and Osipov *et al.*[16] reported changes in the π-plasmon energy of graphite and nanographite structures due to varying L_a. In this article, we present the effects of disorder on the linear and non-linear optical properties of CVD grown graphene. We provide an empirical relation for the π-plasmon energy in terms of L_a, and discuss the influence of L_a on its excitonic lineshape in the optical absorption spectra of

[a]*Department of Physics and Astronomy, Clemson University, Clemson, SC, 29634, USA*
[b]*Department of Physics, Sri Sathya Sai Institute of Higher Learning, Prashanti Nilayam, Andhra Pradesh, 515134, India*
[c]*Light and Matter Physics Group, Raman Research Institute, C V Raman Avenue, Sadashivanagar, Bangalore, 560080, India*
[d]*Center for Optical Materials Science and Engineering Technologies, Clemson University, Clemson, SC, 29634, USA. E-mail: arao@clemson.edu*

† Electronic supplementary information (ESI) available. See DOI: 10.1039/c2nr11206j

polycrystalline graphene. In addition, saturable absorption properties of these samples, probed using the open aperture Z-scan measurements, indicate that the saturation intensity varies linearly as a function of L_a.

Experimental

The graphene samples used in this study were grown on Cu substrates using the CVD technique, and subsequently transferred to 1 mm thick quartz substrates using the procedure described in ref. 18. Briefly, Cu foils (1 cm × 1 cm) were placed in a 1″ quartz tube furnace and heated to 1000 °C in the presence of 50 sccm of H_2 and 450 sccm of Ar. Next, methane at different flow rates (1–8 sccm) was introduced into the furnace for 20–30 min. The samples were finally cooled to room temperature under flowing H_2, Ar and CH_4. To transfer the graphene layers to the quartz substrates, the Cu substrates were spin-coated with PMMA (diluted with 4% anisole) at 4000 rpm followed by a heat treatment for 5 min at 150 °C. Graphene attached to the PMMA layer was obtained by etching the Cu foil using Transene Inc., CE-100 etchant, and carefully washing in 10% HCl and de-ionized water for 10 min. Finally, the samples were transferred to 1 mm thick quartz substrates and annealed at 450 °C in Ar (300 sccm) and H_2 (700 sccm) for 2 h to remove the residual PMMA.

A Perkin-Elmer Lambda 950 UV-Vis spectrometer was used for obtaining the optical absorption spectra of the graphene samples transferred to quartz substrates. As grown graphene samples were also transferred to holey carbon/Cu grids as described in ref. 19 for transmission electron microscopy (TEM) and electron diffraction studies. Hitachi HD-9500 and H-7600 electron microscopes were used for detailed TEM studies. A Dilor XY triple grating monochromator was used for collecting the micro-Raman (using 100× objective) spectra of all samples with the 514.5 nm excitation from an Ar^+ ion laser.

The nonlinear transmission of our samples (transferred to the quartz substrate) in the nanosecond excitation regime was obtained in an open aperture Z-scan configuration (see the ESI, Fig. S1†) using the following linearly polarized pulses from a Q-switched frequency-doubled Nd:YAG laser: (i) 5 ns excitation at 532 nm (20 μJ) and (ii) 7 ns excitation at 1064 nm (30 μJ). Details of the Z-scan method are described in the ESI†.

Results and discussion

Micro-Raman spectroscopy

As evident in Fig. 1a, all CVD grown graphene samples exhibit strong D- and G-bands. The D-band observed at ~1350 cm^{-1} confirms the polycrystalline nature of our samples. The lineshape of the G′-band for the 1 sccm samples is consistent with the Raman spectrum of BLG. Previously, Park *et al.*[20] argued that the origin of the G′-band in BLG (tri-layer graphene or TLG) can be traced to four (nine) possible optical Raman processes. However, only three (five) of such optical processes are non-degenerate. Thus, the Raman spectrum for 1 sccm samples was fitted to 3 Lorentzians consistent with the established peak widths (or phonon life times) for BLG. The lineshape of the G′-band of 2, 4 and 8 sccm samples consists of 3 or more peaks and suggests the existence of 3–5 graphene layers (or FLG).

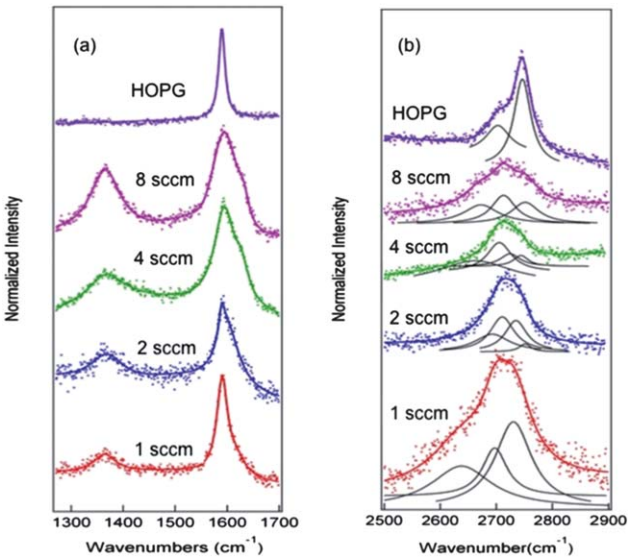

Fig. 1 Room temperature Raman spectra of as-prepared CVD grown graphene samples showing the D- and G-bands (a) and the G′ band (b). The methane flow rates are indicated in both panels. The multi-peak fitting analysis suggests the presence of BLG in 1 sccm samples and FLG in 2, 4 and 8 sccm samples. The top most spectra correspond to the Raman spectra of HOPG. As expected, the D Raman band in HOPG is absent due to its high crystalline order.

Electron microscopy

Fig. 2a and b show typical TEM images of our samples discussed in Fig. 1. The hexagonal electron diffraction pattern along with the TEM images confirms the presence of the polycrystalline nature of our samples. Previously, Huang *et al.*[21] observed varying mean grain size for graphene grown on different Cu foils suggesting that the substrate grain size distribution influences the in-plane crystallinity of CVD grown graphene. Furthermore, recent studies discussing the growth kinetics of graphene (on Cu substrates) suggest a nucleation-based mechanism for graphene formation. The weak interaction between the Cu substrate and graphene was found to result in graphene formation across the grain boundary. However, several defects are often found near the nucleation center (see Fig. 4a in ref. 22) and across the grain boundaries confirming that the defects in the Cu substrate[22] highly influence the value of L_a. In order to further understand the correlation between the graphene crystallinity and the Cu

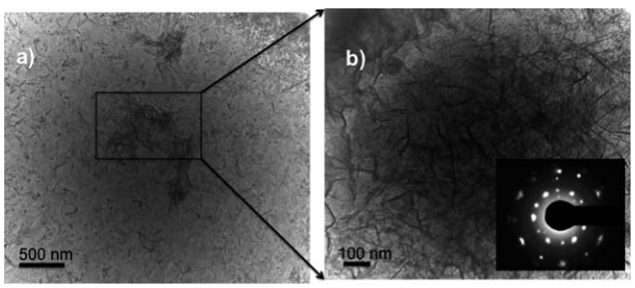

Fig. 2 (a) Typical transmission electron microscope images of CVD grown poly-crystalline graphene. (b) A magnified view of the boxed area in (a). The inset shows hexagonal diffraction pattern obtained from the graphene samples.

grain size, and the ensuing optical properties described below, we used Raman spectroscopy to obtain L_a values for graphene from Cancado's formula.[13]

$$L_a\ (\text{nm}) = 2.4 \times 10^{-10}\ \lambda^4\ (I_G/I_D), \qquad (1)$$

where λ is the excitation wavelength.

The average size and distribution of Cu grains was evaluated by approximating the grain size to the square root of the grain area obtained from the optical images using ImageJ software (see the ESI, Fig. S2†). Interestingly, we find a linear dependence of L_a on the Cu substrate grain size (Fig. 3a), consistent with a previously observed trend of large crystalline metallic substrates favoring larger graphene crystallites.[21] Furthermore, we find that the growth of graphene with lower defects (higher L_a) is favored above a critical Cu grain size of ~40 μm confirming that the crystallinity of the Cu substrate is a crucial factor in the graphene synthesis.

Optical absorption studies

We measured the optical absorption of six different samples (indicated as A–F in Fig. 3a and 4) with different L_a to study the effect of crystalline order on the π-plasmon resonance in graphene. The UV-visible absorption spectrum of graphene exhibits a pronounced resonance at ~4.75 eV (~260 nm) which arises from the electronic transitions near the M-point (from π to π* orbital) in the Brillouin zone of graphene.[22–24] The energy dispersion near the M-point is locally flat (saddle point) and thus leads to a *discrete* van Hove singularity (vHS) in the graphene density of states. The transition occurring slightly below the *M*-point feature (or the vHS in the density of states) is also

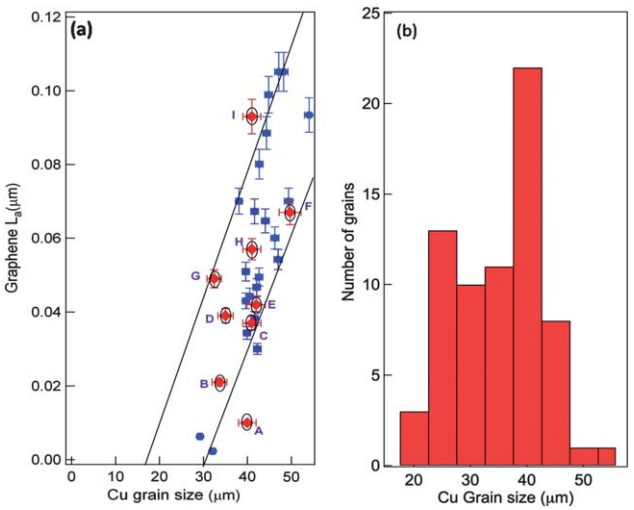

Fig. 3 (a) A map of graphene crystallite size L_a (obtained from micro-Raman spectroscopy) as a function of Cu grain size present in the copper foils used in the CVD synthesis of graphene. The L_a values were obtained by averaging the Raman spectra at 10 different spots. Cu grain sizes were obtained from the optical microscope images of Cu grains using imageJ program. Highlighted areas show the range of dominant Cu grain sizes. Samples indicated A–F (2–5 layers thick) were used for optical absorption studies. The top right hand corner of the plot indicates that high quality graphene (low defects) is obtained when the Cu grain size exceeds ~40 μm. (b) A histogram showing the population of various Cu grain sizes.

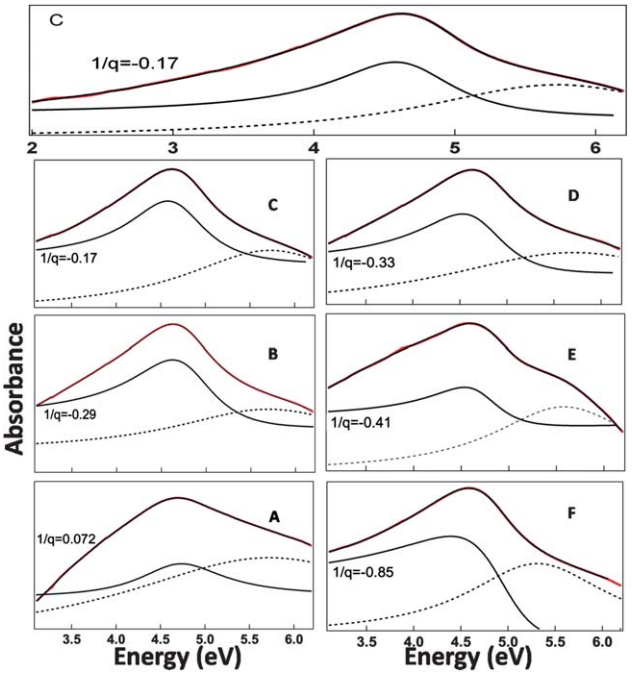

Fig. 4 UV-Visible absorption spectra of graphene samples with different crystallite sizes (for samples A–F indicated in Fig. 3a). Clearly, the peak at ~4.75 eV (260 nm) in the top panel shows the presence of asymmetric Fano lineshape (see text for details). The Lorentzian (shown in dashed lines) slightly above the plasmon energy is the vHS in the density of states as described in ref. 24.

known as π-plasmon in graphite and carbon nanotubes[15,16] and has also been observed in graphene.[23–25] Specifically, Mak *et al.*[23] observed that the optical conductivity of exfoliated graphene deviated significantly from the predicted universal value (~2.3%) within an independent-particle model. However, Mak *et al.* observed only a very slight variation of π-plasmon resonance with layer thickness in few-layer graphene (FLG). In addition, the π-plasmon resonance was also found to exhibit asymmetric Fano line shape (eqn (2)) due to the interaction of the discrete vHS with continuum states near the *K*-point,[23,24,26]

$$I(E) = I_o \frac{\left(1 + (E - E_o/q\Gamma)\right)^2}{\left(1 + (E - E_o/\Gamma)^2\right)}. \qquad (2)$$

In the above equation, I is the intensity, E_o is the resonance frequency, Γ is half-width of the resonance peak and $1/q$ is the Fano interaction parameter.

The π-plasmon energy of graphene is given by[1]

$$h\omega_\pi = \frac{h\omega_p}{2}\left(1 - \frac{4\pi^2 ma^2\gamma_0}{3h^2}\left(1 + \frac{\gamma_1 c^2}{4a^2\gamma_0}\right)\right) \qquad (3)$$

where

$$h\omega_p = \sqrt{\frac{4\pi ne^2}{m}}.$$

a and c are graphene lattice parameters, m is the electron rest mass, n is the carrier concentration and h is Planck's constant, γ_o and γ_1 are overlap integrals. Since the π-plasmon peak results

from the p_z orbitals present in the hexagonal network of carbon atoms, the in-plane defect density (hence L_a) will influence the plasmon energy more significantly than the layer stacking in graphene. We find that the π-plasmon wavelength of our graphene samples varies inversely as a function of L_a (Fig. 5), similar in behavior to that observed in graphite.[15,16]

Following Hashimoto *et al.*[15] we explain the observed changes in the π-plasmon energy of graphene in terms of a change in the carrier concentration (n) due to varying defect density in our polycrystalline graphene samples (eqn (3)). As described in Fig. 4, the peak at 4.75 eV (~260 nm) exhibits a Fano line shape (eqn (2)) due to the interaction with the Dirac continuum states in the vicinity of the K point. We show that the parameter q (in eqn (2)) varies with L_a (inset of Fig. 5); suggesting that the crystallite size influences the interaction between the π-plasmon and the continuum states in graphene. Such changes in the interaction parameter q were previously observed to shift the phonon frequency due to a renormalization process.[26] Thus, we attribute the observed upshift in the π-plasmon energy (or the downshift in wavelength) to changes in the interaction (indicated by q) between the discrete vHS and Dirac continuum states with varying L_a. Further, we find that the π-plasmon wavelength in our data follows an empirical relationship $\lambda_\pi = 250.5\ \text{nm} + 89.5\ \text{nm}^2/L_a$.

Non-linear optical studies

In this final section, we address the effect of L_a on the non-linear optical properties. We observed that the linear optical properties (*i.e.*, the π-plasmon resonance) of our polycrystalline samples saturate for $L_a > 40$ nm albeit the differences in defect density and crystallite size (Fig. 5). Hence we studied our samples with $L_a > 40$ nm (G, H and I) under non-linear excitation to better understand the effect of disorder on their optical properties.

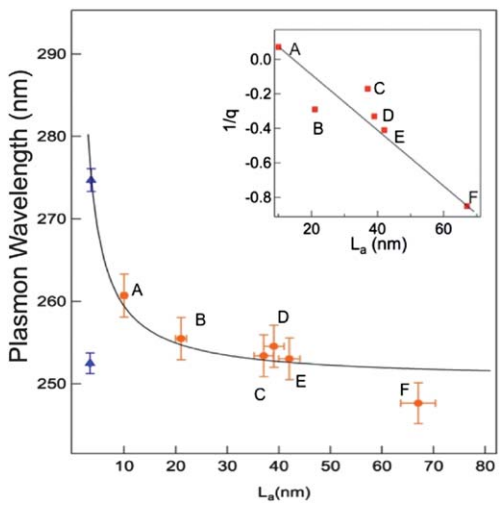

Fig. 5 Dependence of the π-plasmon wavelength on L_a. The curve serves as a guide to the eye. The data points in blue are the plasmon energies for nanographite obtained from ref. 16. The lower wavelength data point (blue triangle ~250 nm) is omitted from the π-plasmon fit as it corresponds to the vHS in the density of states (see dotted peak in Fig. 4) rather than the π-plasmon resonance. The inset shows the variation of interaction parameter as a function of crystallite size.

Fig. 6 shows the Z-scan data obtained for the samples G, H and I (shown in Fig. 3) with ~65% linear transmittance.

Irrespective of the excitation energy used in the experiment, an increase in the normalized transmittance (T) is evident as the samples approach $z = 0$, confirming the presence of saturable absorption in all three samples. It is important to note that in the ns regime, T strongly depends on the excited state population density. Saturable absorption occurs when the absorption cross-section of the excited state is less than that of the ground state. When the samples are excited using a high intensity laser, the increase in the concentration of the photogenerated carriers results in a carrier density that is much larger than the intrinsic carrier density of graphene. Hence there is a rise in T of the system when most of the electrons in the ground state are excited within the width of the incident laser pulse. The saturable absorption occurs since two photoexcited carriers cannot occupy the same state as governed by the Pauli's exclusion principle (known as Pauli blocking).[27,28] The data in Fig. 6 show that our polycrystalline graphene exhibits saturable absorption in the ns region, akin to what has been reported in the literature for graphene oxide.[29] The ns laser pulses excite the carriers in the valence band to generate a non-equilibrium carrier distribution (*via* SA and 2PA in this case) unlike the usual Fermi–Dirac (FD) distribution. This distribution initially broadens into a FD-like distribution with very high temperatures (relative to the lattice) within ~8 to 10 fs due to carrier–carrier scattering,[17,28] and corresponds to the intrinsic carrier relaxation rate. Subsequently, this hot FD-like distribution could decay (in few ps) due to carrier–phonon scattering. Further, such slow decay of carriers may be prolonged (to 100 ps–1 ns) due to the presence of trap states.[29]

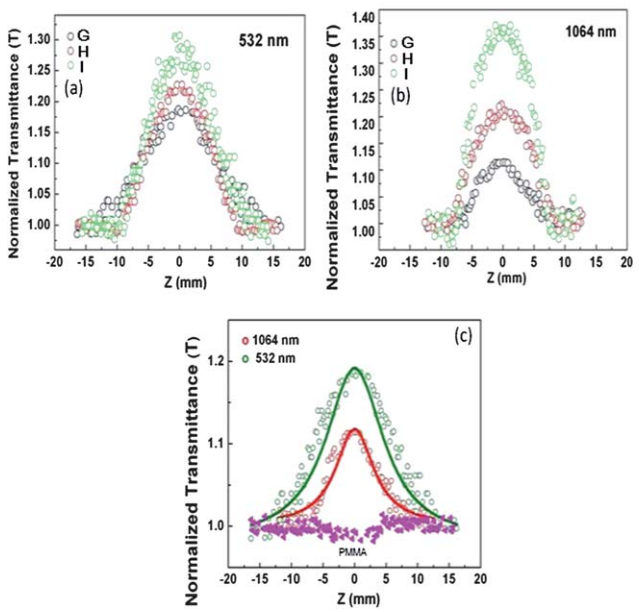

Fig. 6 Open aperture Z-scan data obtained for G, H and I samples using 20 μJ of 5 ns pulses of 532 nm (a) and 30 μJ, 1064 nm (b). Numerical fits obtained from eqn (3) and (4) are shown (c). The bottom most spectrum in (c) corresponds to the Z-scan data for PMMA (using 532 nm excitation) which do not contribute significantly to the graphene spectrum.

It is noteworthy that the saturable absorption process is independent of excitation energy since the energy dispersion of graphene is linear in the vicinity of the K point (*i.e.*, any level in the valence band may be coupled to an appropriate level in the conduction band by the incident photon). Importantly, as explained below, the increase in normalized ΔT is sensitive to the number of graphene layers present in the sample, L_a and the excitation wavelength used in the experiment.

In order to identify the exact nature of the nonlinearity, the Z-scan data were fit to different nonlinear transmission equations, and the best numerical fit was obtained using eqn (4) and (5) (Fig. 6c). Our analyses suggest two possible origins for the observed nonlinearity in the nanosecond excitation regime: (i) a strong saturation of the ground state absorption and (ii) weak two photon absorption (2PA). Therefore, an effective nonlinear absorption coefficient $\alpha(I)$, given by

$$\alpha(I) = \left(\frac{\alpha_0}{1 + I/I_s}\right) + \beta I \tag{4}$$

was considered, where α_0 is the unsaturated linear absorption coefficient at the excitation wavelength, I is the input laser intensity, I_s is the saturation intensity (intensity at which the linear absorption drops to half its original value) and β is the effective 2PA coefficient. The transmitted intensity for a given input fluence is calculated by numerically solving the propagation equation

$$\frac{dI}{dz'} = -\left[\left(\frac{\alpha_0}{1 + I/I_s}\right) + \beta I\right] I \tag{5}$$

Here z' indicates the propagation distance within the sample. The nonlinear parameters β and I_s are determined from the best-fit analysis of the experimental data.

Fig. 7 shows the variation of the effective 2PA coefficient (β) at 532 nm as a function of the $I_{G'}/I_G$. Clearly, β shows a small change as a function of $I_{G'}/I_G$ indicating that the layer stacking does not significantly affect the 2PA coefficient which can be rationalized as follows. It is well known that the linear absorption in graphene is 2.3% for a single layer irrespective of the incident energy.[28] Thus, it is reasonable to expect that the transition probability for the carriers does not change drastically for the samples used in this study.

On the other hand, the saturation intensity (I_s) decreases considerably with a decrease in $I_{G'}/I_G$ for both 532 and 1064 nm (Fig. 7b). In the case of saturation intensity, the effects of layer stacking are two-fold: (i) *effect of excitation:* the longer wavelength at 1064 nm probes the carriers closer to the Fermi level when compared to 532 nm (Fig. 7a). Since the density of states is lower near the Fermi level, longer wavelength excitations result in lower values of I_s for a given number of layers (bottom 2 curves in Fig. 7b). (ii) *Effect of layer stacking:* as discussed in ref. 27, the saturation carrier density (N) may be approximated for a continuous wave excitation using eqn (6).

$$N = \alpha F \tau / \hbar\omega \tag{6}$$

where τ is the recombination time, F is the input fluence and ω is the excitation frequency. Hence, for a given incident excitation and fluence, the saturation carrier density is determined solely by

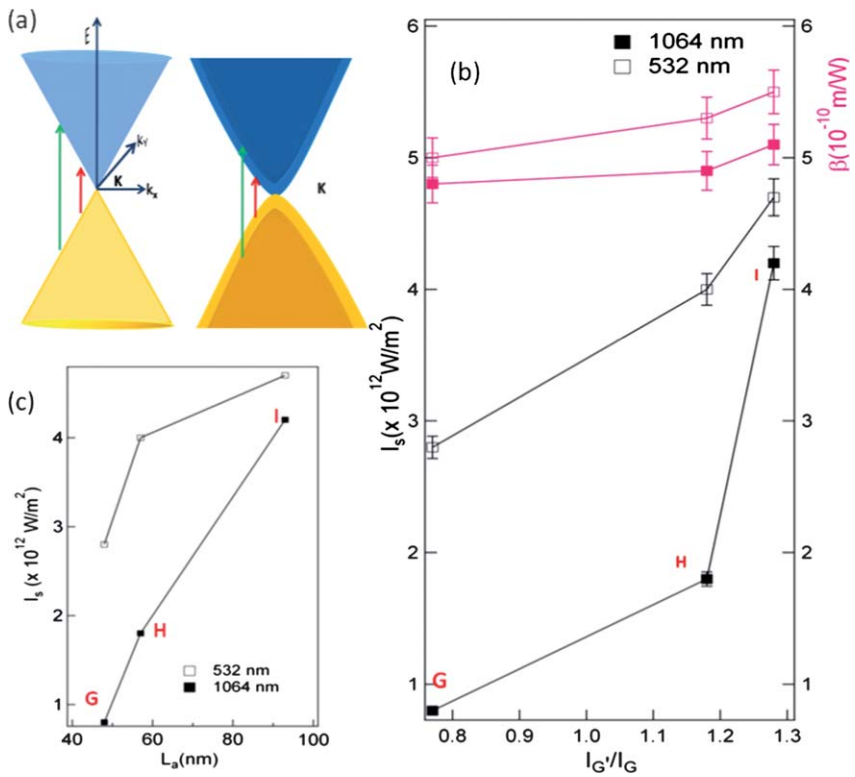

Fig. 7 (a) The electronic energy band structure for SLG and BLG near the K-point. Energy varies nonlinearly with momentum as the layer stacking increases. In addition, the stacked layers result in sub-bands. (b) The variation of 2PA coefficient and saturation intensity (obtained using the fits described in Fig. 6c) as a function of $I_{G'}/I_G$. (c) The variation of saturation intensity as a function of L_a.

the recombination time. The recombination time depends upon the defect density in the given sample and may be correlated to L_a. Dawlaty *et al.*[17] previously observed that for higher values of L_a (or smaller crystal disorder), the photogenerated carriers will have a longer recombination time. Thus, the saturation intensity is expected to vary linearly as a function of L_a. This behavior is observed in Fig. 7c indicating that the saturation intensity in our samples occurs due to different recombination times (or crystallite size).

Conclusion

In summary, we observed that the π-plasmon energy of graphene shows renormalization effects due to Fano resonance near the M-point. The crystallite size strongly influences the π-plasmon energy *via* the interaction between discrete vHS and Dirac continuum. Furthermore, we showed that the layer stacking in graphene has no significant effects on the effective two-photon absorption coefficient. The saturation intensity, in the Z-scan experiments, was observed to vary both as a function of the incident energy and crystallite size indicating that it is sensitive to the changes in the graphene domain size.

Acknowledgements

The authors thank Prof. M. J. Skove and Dr Jian He (Clemson University) and Dr Rahul Rao (WPAFB, Ohio) for their valuable discussion and suggestion. The authors acknowledge Dr Haijun Qian for his help with H-9500 TEM measurements. BA and SSSS acknowledge the financial support from UGC and DST, India.

References

1 K. S. Novoselov, A. K. Geim, S. V. Morozov, D. Jiang, M. I. Katsnelson, I. V. Grigorieva, S. V. Dubonos and A. A. Firsov, *Nature*, 2005, **438**(7065), 197–200.
2 Y. Zhang, T.-T. Tang, C. Girit, Z. Hao, M. C. Martin, A. Zettl, M. F. Crommie, Y. R. Shen and F. Wang, *Nature*, 2009, **459**(7248), 820–823.
3 S. Latil, V. Meunier and L. Henrard, *Phys. Rev. B: Condens. Matter Mater. Phys.*, 2007, **76**(20), 201402.
4 Z. Ni, Y. Wang, T. Yu, Y. You and Z. Shen, *Phys. Rev. B: Condens. Matter Mater. Phys.*, 2008, **77**(23), 235403.
5 A. C. Ferrari, J. C. Meyer, V. Scardaci, C. Casiraghi, M. Lazzeri, F. Mauri, S. Piscanec, D. Jiang, K. S. Novoselov, S. Roth and A. K. Geim, *Phys. Rev. Lett.*, 2006, **97**, 187401.
6 A. Gupta, G. Chen, P. Joshi, S. Tadigadapa and P. Eklund, *Nano Lett.*, 2006, **6**(12), 2667–2673.
7 L. Cançado, A. Reina, J. Kong and M. Dresselhaus, *Phys. Rev. B: Condens. Matter Mater. Phys.*, 2008, **77**(24), 245408.
8 L. Malard, M. Pimenta, G. Dresselhaus and M. Dresselhaus, *Phys. Rep.*, 2009, **473**(5–6), 51–87.
9 A. K. Gupta, Y. Tang, V. H. Crespi and P. C. Eklund, *Phys. Rev. B: Condens. Matter Mater. Phys.*, 2010, **82**, 241406(R).
10 R. Rao, R. Podila, R. Tsuchikawa, J. Katoch, D. Tishler, A. M. Rao and M. Ishigami, *ACS Nano*, 2011, **5**(3), 1594.
11 C. Cong, T. Yu, R. Saito, G. F. Dresselhaus and M. S. Dresselhaus, *ACS Nano*, 2011, **5**(3), 1600.
12 M. A. Pimenta, G. Dresselhaus, M. S. Dresselhaus, L. G. Cancado, A. Jorio and R. Saito, *Phys. Chem. Chem. Phys.*, 2007, **9**, 1276.
13 L. G. Cancado, K. Takai, T. Enoki, M. Endo, Y. A. Kim, S. Mizusaki, A. Jorio, L. N. Coehlo, M.-R. Paniago and M. A. Pimenta, *Appl. Phys. Lett.*, 2006, **88**, 3106.
14 D. S. Knight and W. B. White, *J. Mater. Res.*, 1989, **4**, 385.
15 H. Hashimoto, S. Nishiuma, K. Takada, K. Nakamura, R. Ueno and T. Den, *Jpn. J. Appl. Phys.*, 1999, **38**, 4136.
16 V. Y. Osipov, A. V. Baranov, V. A. Ermakov, T. L. Makarova, L. F. Chungong, A. I. Shames, K. Takai, T. Enoki, Y. Kaburagi, M. Endo and A. Y. Vul', *Diamond Relat. Mater.*, 2011, **20**, 205.
17 J. M. Dawlaty, S. Shivaraman, M. Chandrashekhar, F. Rana and M. G. Spencer, *Appl. Phys. Lett.*, 2008, **92**(4), 042116.
18 S. Bhaviripudi, X. Jia, M. S. Dresselhaus and J. Kong, *NanoLett.*, 2010, **10**(10), 4128.
19 W. Regan, N. Alem, B. Aleman, B. Geng, C. Girit, L. Maserati, F. Wang, M. Crommie and A. Zettl, *Appl. Phys. Lett.*, 2010, **96**, 113102.
20 J. S. Park, A. Reina, R. Saito, J. Kong, G. Dresselhaus and M. S. Dresselhaus, *Carbon*, 2009, **47**, 1303.
21 Y. P. Huang, C. S. Ruiz-Vargas, A. M. van der Zande, W. S. Whitney, M. P. Levendorf, J. W. Kevek, S. Garg, J. S. Alden, C. J. Hustedt, J. Park, P. L. McEuen and D. A. Muller, *Nature*, 2011, **469**, 389.
22 Q. Yu, L. A. Jauregui, W. Wu, R. Colby, J. Tian, Z. Su, H. Cao, Z. Liu, D. Pandey, D. Wei, T. F. Chung, P. Peng, N. P. Guisinger, E. A. Stach, J. Bao, S.-S. Pei and Y. P. Chen, *Nat. Mater.*, 2011, **10**, 443.
23 K. F. Mak, J. Shan and T. F. Heinz, *Phys. Rev. Lett.*, 2011, **106**, 046401.
24 D.-H. Chae, T. Utikal, S. Weisenburger, H. Giessen, K. V. Klitzing, M. Lippitz and J. Smet, *Nano Lett.*, 2011, **11**, 1379.
25 K. Lingam, R. Podila, C. Loebick, P. Chen, P.-C. Ke, B. Powell, L. Pfefferle and A. M. Rao, *Carbon*, 2011, **49**, 3803.
26 A. M. Rao, P. C. Eklund, S. Bandow, A. Thess and R. E. Smalley, *Nature*, 1997, **388**, 257.
27 Q. Bao, H. Zhang, Y. Wang, Z. Ni, Y. Yan, Z. X. Shen, K. P. Loh and D. Y. Tang, *Adv. Funct. Mater.*, 2009, **19**, 3077.
28 G. Xing, H. Guo, X. Zhang, T. C. Sum and C. H. Alfred Huan, *Opt. Express*, 2010, **18**(5), 4564.
29 G.-K. Lim, Z.-L. Chen, J. Clark, R. G. S. Goh, W.-H. Ng, H.-W. Tan, R. H. Friend, P. K. H. Ho and L.-L. Chua, *Nat. Photonics*, 2011, **5**, 554.